 Bull. Chem. Soc. Jpn. Vol. 81, No. 6, 697–702 (2008)

Monte Carlo Study of First-Order Phase Transitions of a Bulk Lennard–Jones Fluid System in the Isobaric–Multithermal Ensemble

Chizuru Muguruma*[1] and Yuko Okamoto[2]

[1]Faculty of Liberal Arts, Chukyo University, Toyota 470-0393

[2]Department of Physics, Nagoya University, Nagoya 464-8602

Received September 3, 2007; E-mail: muguruma@lets.chukyo-u.ac.jp

A Monte Carlo (MC) simulation in the isobaric–multithermal (MUTH) ensemble has been carried out for a bulk Lennard–Jones fluid system that consists of 108 particles to investigate the validity of the algorithm. After we obtain the best estimate of the MUTH (isobaric–multithermal) weight factor, the probability distributions, the expectation values of some physical quantities, and the radial distribution functions are calculated for the temperature range between $T^* = 0.417$ and 1.00 under the pressure of $P^* = 2.42 \times 10^{-3}$ from the MUTH MC production run by adopting reweighting techniques. The thermodynamic quantities exhibit the characteristics of first-order phase transitions at $T^* = 0.726$, which correspond to the transition from face-centered-cubic (f.c.c.) solid to liquid by judging from the radial distribution functions and the snapshots. The obtained contour representation of the probability distribution at $T^* = 0.726$ and $P^* = 2.42 \times 10^{-3}$ shows two distinct configurational spaces. The changes in thermodynamic quantities at the phase-transition temperature of Lennard–Jones argon (at 87 K under 1 atm) were also compared with those of real argon.

Conventional canonical simulations of complex systems tend to get trapped at low temperatures in local minimum states on the potential energy surface. The multicanonical (MUCA) algorithm[1,2] has been introduced in order to overcome this multiple-minima problem and has been applied to study first-order phase transitions[1–16] (for recent reviews, see Refs. 17 and 18). The algorithm is based on an artificial, non-Boltzmann weight factor and performs a free one-dimensional random walk in potential energy space, which allows the simulation to avoid getting trapped in states of energy local minima. Moreover, one can calculate the expectation values of thermodynamic quantities as functions of temperature by applying single-histogram reweighting techniques[19] to the results of one long production run.

A Lennard–Jones fluid system, such as an argon fluid, is a typical system with first-order phase transitions.[7,10,20,21] We have investigated the phase transition of the Lennard–Jones fluid by using the MUCA MC method.[15,16] One of the problem of this method is that the pressure of the system changes as temperature varies because the number of particles and volume are fixed in the MUCA ensemble. Besides, most of the experimental data is obtained under constant pressure, typically under 1 atm. To expand the features of the MUCA algorithm, three generalized isobaric–isothermal algorithms, which are named as the multibaric–multithermal (MUBATH), multibaric–isothermal (MUBA), and isobaric–multithermal (MUTH) algorithms, are proposed in Refs. 22–24.

Among them, the MC simulation in the isobaric–multithermal ensemble is suitable to obtain thermodynamic quantities comparable to experimental data. In the present study, we apply the MUTH MC method to the Lennard–Jones fluid system, investigate the changes in thermodynamic quantities across the phase-transition point under $P^* = 2.42 \times 10^{-3}$ (1 atm for the Lennard–Jones argon system), and the gaps in thermodynamic quantities at the phase-transition point are compared with the experimental data.

This article is organized as follows. In section II, the MUTH MC method is briefly described. We report the results of the MUTH MC simulation of a bulk argon system in section III. Conclusions follow in section IV.

Computational Methods

MUTH Ensemble. Although the MUTH algorithm, that is an extension of multicanonical algorithm to the isobaric–multithermal ensemble, is explained elsewhere,[23] we give a short overview in this subsection for completeness. In NPT ensemble the probability distribution $\mathrm{P}_{\mathrm{NPT}}(E, V; T_0, P_0)$ of the potential energy E and volume V at temperature T_0 and pressure P_0 is given by the product of the density of states $n(E, V)$ and the NPT weight factor $w_{\mathrm{NPT}}(E, V; T_0, P_0)$:

$$\begin{aligned} \mathrm{P}_{\mathrm{NPT}}(E, V; T_0, P_0) &\propto n(E, V) w_{\mathrm{NPT}}(E, V; T_0, P_0) \\ &= n(E, V) \exp[-\beta_0 (E + P_0 V)], \end{aligned} \tag{1}$$

where β_0 is the inverse temperature $1/k_{\mathrm{B}}T_0$ with the Boltzmann constant k_{B}. Since $n(E, V)$ is a rapidly increasing function and $w_{\mathrm{NPT}}(E, V; T_0, P_0)$ decreases exponentially, $\mathrm{P}_{\mathrm{NPT}}(E, V; T_0, P_0)$ generally has a bell-like shape.

In the MUTH ensemble each state is weighted by a non-Boltzmann weight factor $w_{\mathrm{MUTH}}(E)$, which we refer to as the MUTH weight factor, so that a uniform potential energy distribution may be obtained:

Published on the web June 11, 2008; doi:10.1246/bcsj.81.697

$$\int \mathrm{d}V \mathrm{P}_{\mathrm{MUTH}}(E,V;P_0) \propto \int \mathrm{d}V n(E,V)\exp(-\beta_0 P_0 V) w_{\mathrm{MUTH}}(E) \equiv \text{constant}. \quad (2)$$

The flat artificial energy distribution implies that a one-dimensional free random walk in the potential energy space is realized. The random walk allows the system to escape from any local-minimum-energy states and to sample the configurational space much more widely with a smaller number of simulation steps than conventional MC or molecular dynamics methods.

According to the definition in eq 2, the MUTH weight factor $w_{\mathrm{MUTH}}(E)$ is determined by the density of the states $n(E,V)$ at each potential energy E and can be written as follows:

$$w_{\mathrm{MUTH}}(E) = \frac{1}{\int \mathrm{d}V n(E,V)\exp(-\beta_0 P_0 V)}. \quad (3)$$

The MUTH weight factor, as well as the multicanonical weight factor, has to be determined numerically by iterations of short preliminary runs because the density of states of the system is usually unknown. In the present study, we employed the iterative procedure in Ref. 25 as well as single-histogram[19] and multiple-histogram[26,27] reweighting techniques.

A MUTH MC simulation is performed, for instance, with the usual Metropolis criterion:[28] The transition probability of state x with potential energy E and volume V to state x' with potential energy E' and volume V' is given by

$$w(x \to x') = \begin{cases} 1, & \text{for } \Delta W \le 0, \\ \exp(-\Delta W), & \text{for } \Delta W > 0, \end{cases} \quad (4)$$

where

$$\Delta W \equiv \ln \frac{w_{\mathrm{MUTH}}(E)}{w_{\mathrm{MUTH}}(E')} + \beta_0 P_0 (V' - V) - N \ln\left(\frac{V'}{V}\right). \quad (5)$$

Once the MUTH weight factor is given, one performs a long MUTH production run. By tracing the potential energy surface during the simulation, the global-minimum energy state can be identified. Moreover, adopting the reweighting techniques, the probability distribution $\mathrm{P}_{\mathrm{NPT}}(E,V;T,P)$ and the expectation value of a physical quantity θ at any temperature T $(=1/k_{\mathrm{B}}\beta)$ and pressure P are given by

$$\mathrm{P}_{\mathrm{NPT}}(E,V;T,P) = \frac{\mathrm{P}_{\mathrm{MUTH}}(E,V;P_0) w_{\mathrm{MUTH}}^{-1}(E)\exp(\beta_0 P_0 V)\exp[-\beta(E+PV)]}{\int \mathrm{d}E \int \mathrm{d}V \mathrm{P}_{\mathrm{MUTH}}(E,V;P_0) w_{\mathrm{MUTH}}^{-1}(E)\exp(\beta_0 P_0 V)\exp[-\beta(E+PV)]}, \quad (6)$$

and

$$\langle\theta\rangle_{\mathrm{NPT}} = \frac{\int \mathrm{d}E \int \mathrm{d}V \theta(E,V)\mathrm{P}_{\mathrm{NPT}}(E,V;T,P)}{\int \mathrm{d}E \int \mathrm{d}V \mathrm{P}_{\mathrm{NPT}}(E,V;T,P)}, \quad (7)$$

respectively.

Computational Details. We put 108 particles in a cubic cell with periodic boundary conditions. A pair of particles with distance r_{ij} interact through the Lennard–Jones pair potential

$$\upsilon^{lj}(r_{ij}) = 4\varepsilon\left[\left(\frac{\sigma}{r_{ij}}\right)^{12} - \left(\frac{\sigma}{r_{ij}}\right)^{6}\right]. \quad (8)$$

These interactions are truncated at r_{c} which is a half length of the edge size L $(r_{\mathrm{c}} = \frac{L}{2})$:

$$\upsilon(r) = \begin{cases} \upsilon^{lj}(r), & \text{for } r \le r_{\mathrm{c}}, \\ 0, & \text{for } r > r_{\mathrm{c}}. \end{cases} \quad (9)$$

Thus, the total potential energy of the system that consists of N particles is given by

$$E = \sum_{i=1}^{N-1}\sum_{j>i}^{N} \upsilon(r) + E_N^{\mathrm{c}}, \quad (10)$$

Here, the contribution of the particles beyond the truncation at r_{c} in the potential energy is corrected by the following equation:

$$E_N^{\mathrm{c}} = 2\pi N\rho \int_{r_{\mathrm{c}}}^{\infty} 4\varepsilon\left[\left(\frac{\sigma}{r}\right)^{12} - \left(\frac{\sigma}{r}\right)^{6}\right] r^2 \mathrm{d}r = \frac{8}{9}\pi N\sigma^3\rho\varepsilon\left[\left(\frac{\sigma}{r_{\mathrm{c}}}\right)^{9} - 3\left(\frac{\sigma}{r_{\mathrm{c}}}\right)^{3}\right], \quad (11)$$

where ρ is the number density.

Hereafter, the length and the energy are scaled in units of the Lennard–Jones diameter σ and the depth of the potential

Table 1. The Translation of Reduced Units to Real Units for Lennard–Jones Argon

Quantity	Reduced units		Real units
Energy	$E^* = 1$	$\leftrightarrow$	$E = 0.9961\,\mathrm{kJ\,mol^{-1}}$
Distance	$r^* = 1$	$\leftrightarrow$	$r = 3.405\,\text{Å}$
Temperature	$T^* = 1$	$\leftrightarrow$	$T = 119.8\,\mathrm{K}$
Volume	$V^* = 1$	$\leftrightarrow$	$V = 39.48\,\text{Å}^3$
Pressure	$P^* = 2.418 \times 10^{-3}$	$\leftrightarrow$	$P = 1\,\mathrm{atm}$

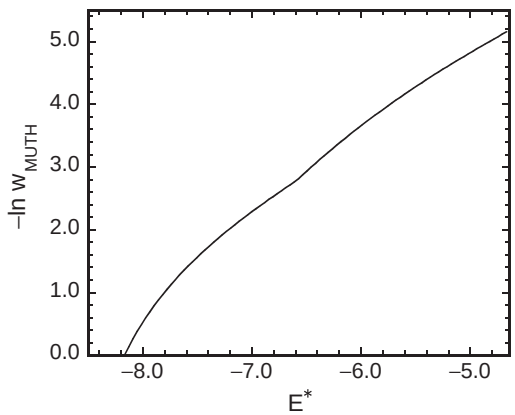

Figure 1. The logarithm of the MUTH weight factor as a function of total potential energy obtained by the MUTH MC production run. We have set $w_{\mathrm{MUTH}}(E^*) = 1$ at $E^* = -8.17$.

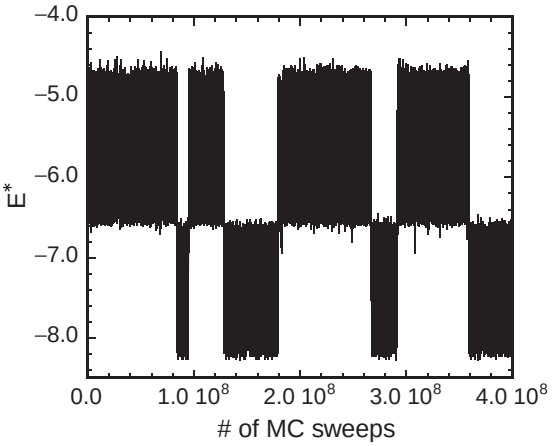

Figure 2. Time series of total potential energy obtained by a long production run of the MUTH MC simulation.

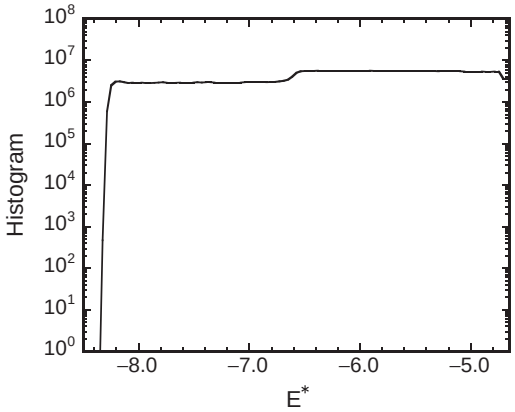

Figure 3. Histogram of the total potential energy distribution that was obtained by the MUTH MC production run.

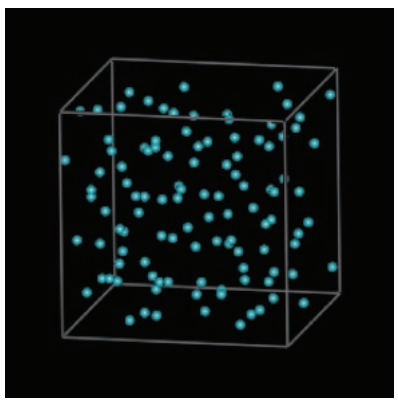

(a)

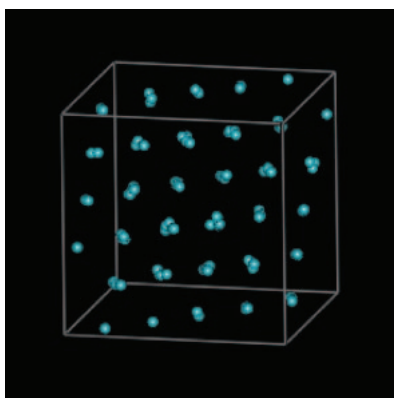

(b)

Figure 4. Snapshots obtained by the MUTH MC production run. The total potential energy is (a) $E^* = -5.46$ and (b) $E^* = -7.81$, respectively. Pictures are the projection along a crystal axis. The mass of particles are observed in the snapshot (b) because of the fluctuation.

ε, respectively. We use in asterisk (*) for the reduced quantities such as the reduced energy $E^* = E/\varepsilon$, the reduced length $r^* = r/\sigma$, the reduced temperature $T^* = k_B T/\varepsilon$, the reduced volume $V^* = V/\sigma^3$, and the reduced pressure $P^* = P\sigma^3/\varepsilon$.

To make a comparison between the calculated results and the experimental data of real argon under 1 atm, we adopt the potential parameters of argon as $\varepsilon/k_B = 119.8\,\mathrm{K}$ and $\sigma = 3.405\,\text{Å}$.[29] The translation of reduced units to real units for Lennard–Jones argon is listed in Table 1. The MUTH MC simulation is carried out under the initial pressure of $P_0^* = 2.42 \times 10^{-3}$ and the MUTH weight factor was determined for the energy range below $E^* = -4.69$ that corresponds to $T^* \leq 1.00$.

Thermodynamic quantities were calculated by the reweighting techniques in eqs 6 and 7. For instance, heat capacity C_P^* was calculated from the following equation:

$$C_P = \frac{\langle H^{*2}\rangle_{NPT} - \langle H^*\rangle_{NPT}{}^2}{T^{*2}}, \tag{12}$$

where the enthalpy H^* is given by $H^* = E^* + P^*V^*$.

Calculating free energy and entropy by ordinary molecular simulation methods requires a lot of effort. However, the Gibbs free energy G^* at temperature T^* ($=\beta^{*-1}$) and pressure P^* can be easily obtained by the following equation:

$$G^*(T^*, P^*) = -\beta^{*-1} \ln Z. \tag{13}$$

where Z is the partition function and is expressed as

$$\begin{aligned} Z &= \int \mathrm{d}E^* \int \mathrm{d}V^* n(E^*, V^*) \exp[-\beta^*(E^* + P^*V^*)] \\ &= \int \mathrm{d}E^* \int \mathrm{d}V^* \mathrm{P}_{MUTH}(E^*, V^*; P_0^*) w_{MUTH}^{-1}(E^*) \\ &\quad \times \exp(\beta_0^* P_0^* V^*) \exp[-\beta^*(E^* + P^*V^*)]. \end{aligned} \tag{14}$$

in the MUTH algorithm. Entropy is also one of the physical quantities that are difficult to calculate by ordinary computer simulation methods. The entropy in the NPT ensemble at temperature T^* and pressure P^* is simply calculated by the relation $G^* = H^* - T^*S^*$:

$$S(T^*, P^*) = -\frac{G^*(T^*, P^*) - H^*(T^*, P^*)}{T^*}, \tag{15}$$

where $H^*(T^*, P^*) = \langle H^*\rangle_{NPT}$, and the reweighting formulae in eqs 6 and 7 were used with $\theta = H^*$.

One MC sweep is defined to consist of 108 coordinate updates of a randomly chosen particle and a random volume change with the Metropolis evaluation for each update. The simulated results are a little sensitive to the number of particles, and the system size of 108 particles is rather small. How-

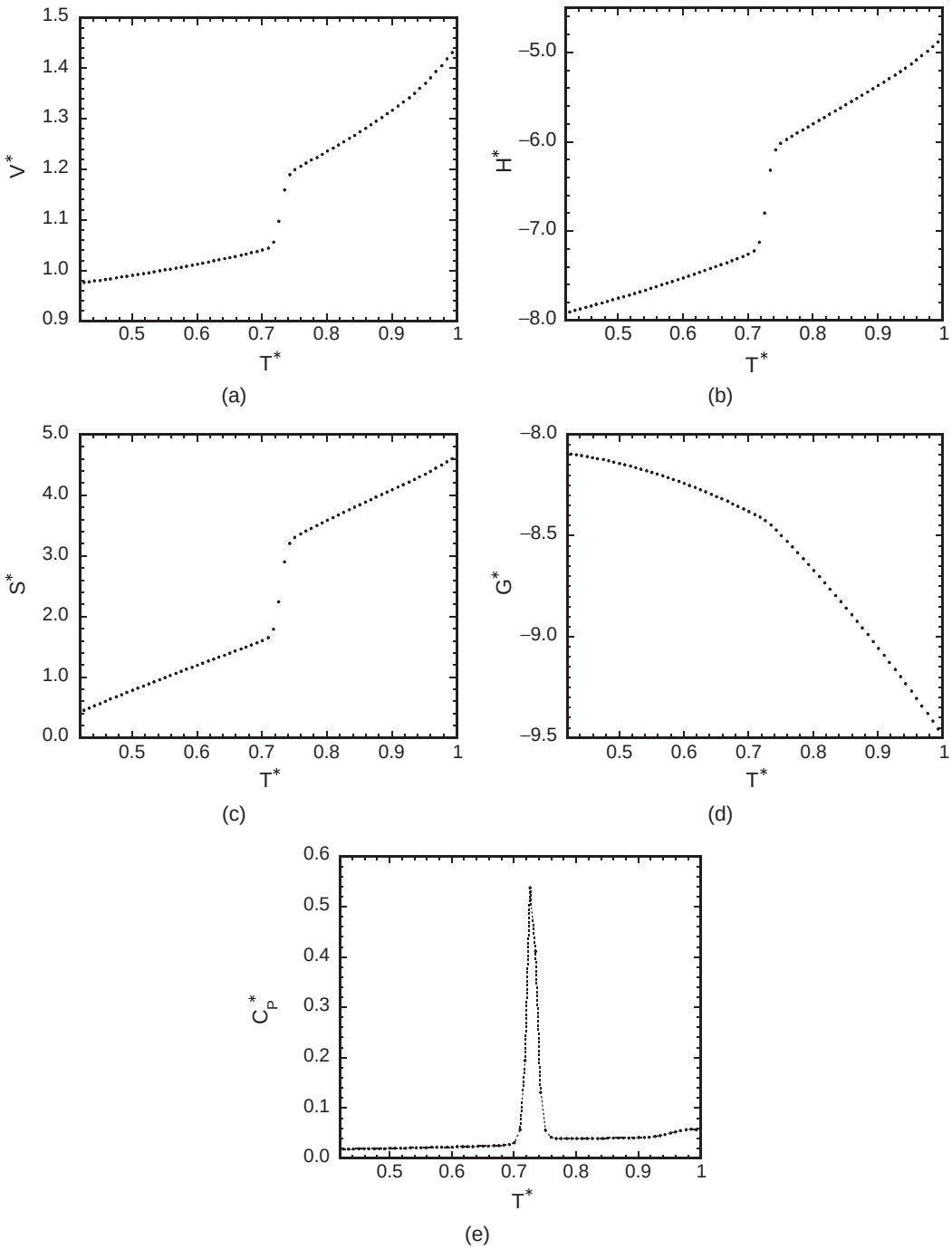

Figure 5. Thermodynamic quantities obtained from the MUTH MC production run by the reweighting techniques (a) average volume, (b) enthalpy, (c) entropy, (d) Gibbs free energy, and (e) heat capacity. The expectation values were calculated at every $T^* = 8.35 \times 10^{-3}$ from 0.417 to 1.00 under $P^* = 2.42 \times 10^{-3}$.

ever, it still satisfied our purpose of testing the validity of our simulation algorithm. All calculations were performed with our own computer code.

Results and Discussion

The MUTH Production Run. Figure 1 shows the logarithm of the MUTH weight factor as in eq 3. The "time series" of total potential energy from the MUTH MC production run is shown in Figure 2. We indeed see a random walk between $E^* = -8.22$ and -4.62. The energy region is divided around $E^* = -6.58$ into two parts, and significant transitions between these two regions takes place at least 7 times during the MUTH MC production run. Figure 3 shows the histogram that was obtained by the MUTH MC production run. We observe a flat histogram in the energy region between $E^* = -8.23$ and -4.69. The MUTH ensemble is realized in this energy region.

Snapshots obtained from the MUTH MC production run are shown in Figure 4. In the higher energy state of Figure 4a, particles are scattered randomly, whereas particles are almost regularly arranged in the lower energy state of Figure 4b.

Therefore we consider that the high-energy state corresponds to the liquid state and the low-energy state to the solid state.

Thermodynamic Quantities. The thermodynamic quantities were calculated as the expectation values of physical quantities at every $T^* = 8.35 \times 10^{-3}$ from 0.417 to 1.00 under $P^* = 2.42 \times 10^{-3}$, which corresponds to every 1 K from 50 to 120 K under 1 atm for Lennard–Jones argon. Average volume, enthalpy, entropy, Gibbs free energy, and heat capacity are shown in Figure 5, which were obtained from the MUTH MC production run by the reweighting techniques in eqs 6 and 7. Average volume, enthalpy, and entropy have a discontinuous change at $T^* = T_c^* = 0.726$ as shown in Figures 5a, 5b, and 5c. Gibbs free energy is shown in Figure 5d. The change in the slope is observed at T_c^*. Heat capacity, shown in Figure 5e, shows a significant peak at the phase-transition temperature. This suggests that the first-order phase transition takes place at this temperature.

Because 1 atm equals to 1.013×10^5 Pa, the results of our calculations are comparable to the experimental data under 10^5 Pa. The "discontinuities" in each thermodynamic quantity at the transition temperature $T_c^* = 0.726$ (87 K) are $\Delta V^* = 0.144$ (5.70 Å^3) for average volume (see Figure 5a), $\Delta H^* = 1.13$ (1.13 kJ mol^{-1}) for enthalpy (see Figure 5b), and $\Delta S^* = 12.9$ (12.8 J mol^{-1} K^{-1}) for entropy (see Figure 5c). On the other hand, the standard enthalpy of fusion at 10^5 Pa is $\Delta_{fus}H^{\ominus} = 1.188$ kJ mol^{-1} and the standard entropy of fusion at 10^5 Pa is $\Delta_{fus}S^{\ominus} = 14.17$ J mol^{-1} K^{-1} at the transition temperature of 83.8 K in the experimental data.[30] We remark that the discontinuities in enthalpy and in entropy at the phase transition point satisfy the thermodynamic relation $\Delta S = \Delta H/T$ both in the simulation results, $((\Delta S, \Delta H/T) = (12.8$ J mol^{-1} K^{-1}, 13.0 J mol^{-1} K^{-1})), and in the experimental results, $((\Delta S, \Delta H/T) = (14.17$ J mol^{-1} K^{-1}, 14.2 J mol^{-1} K^{-1})). The calculated transition temperature is overestimated by 3 K and the discontinuities in the thermodynamic quantities are underestimated slightly.

In order to confirm what kind of transition takes place, the radial distribution functions (RDFs), shown in Figure 6, were calculated at $T^* = 0.417$ and 0.835 from the MUTH MC production run by the reweighting techniques. We observe four peaks at $r^* = 1.10$, 1.62, 1.94, and 2.23 in the RDF at $T^* = 0.417$ and two peaks at $r^* = 1.10$ and 2.20 in the RDF at $T^* = 0.835$. This implies that the transition takes place between liquid and solid states and the solid state is in f.c.c. crystal form.

Probability Distributions. The contour map of the probability distribution $P_{MUTH}(E^*, V^*; P_0^*)$ is shown in Figure 7. The volume size does not spread over the whole volume space but varies as the potential energy changes because the system is restricted by the initial pressure of $P^* = 2.42 \times 10^{-3}$ during the simulation. A significant change in the volume space accompanied with the phase transition is not observed in the present study.

Figure 8 shows the contour map of the reweighted probability distribution at $T^* = 0.417$ and 0.835 under $P^* = 2.42 \times 10^{-3}$. We can observe a broad configurational space at $T^* = 0.835$ and a narrow configurational space at $T^* = 0.417$. The contour map of the reweighted probability distribution at T_c^* is shown in Figure 9. We can observe two minima

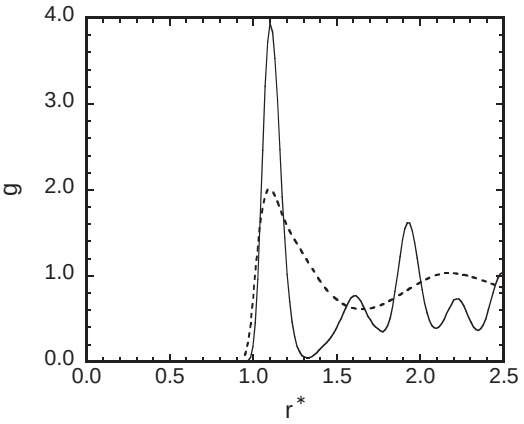

Figure 6. The radial distribution functions at $T^* = 0.417$ and 0.835 under $P^* = 2.42 \times 10^{-3}$, which were obtained from the MUTH MC production run by the reweighting techniques. The RDF at $T^* = 0.417$ is in solid line, and that at $T^* = 0.835$ is in dashed line.

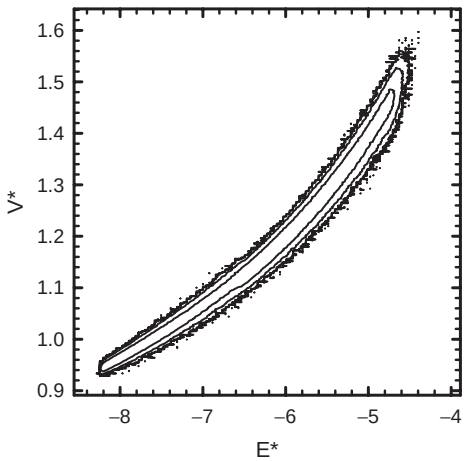

Figure 7. The contour representation of the probability distribution $P_{MUTH}(E^*, V^*; P_0^*)$ in logarithmic scale that was obtained by the MUTH MC production run. The curves are the counter map of $\ln P_{MUTH}(E^*, V^*; P_0^*) = -8$, -10, -12, and -14 and the outermost curve corresponds to -14.

at $E^* = -7.17$ and $V^* = 1.05$ and at $E^* = -6.10$ and $V^* = 1.18$. We can locate the transition state at the saddle point between the two minima, which is at $E^* = -6.60$ and $V^* = 1.10$.

Concluding Remarks

The MUTH algorithm is a powerful simulation method to overcome the multiple-minima problem in the NPT ensemble. We can calculate the expectation values of a physical quantity at any temperature under constant pressure from one MUTH MC production run by reweighting techniques. In the present work, we applied the MUTH MC method to a bulk argon system for $P_0^* = 2.42 \times 10^{-3}$. We observed 7 phase transition events between liquid and solid phases during a single MUTH MC production run, which cannot be accomplished by conventional NPT simulations. The physical quan-

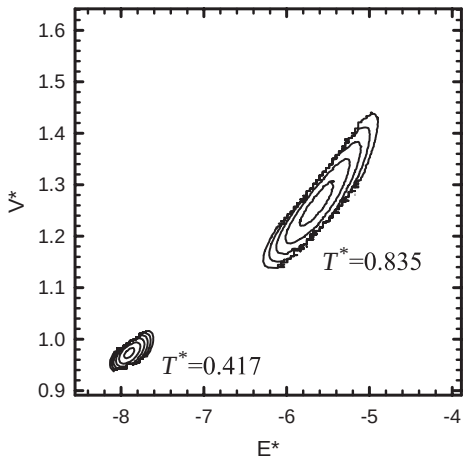

Figure 8. The contour representation of the probability distributions $P_{NPT}(E^*, V^*; T^*, P^*)$ in logarithmic scale at $T^* = 0.417$ and 0.835 under $P^* = 2.42 \times 10^{-3}$ that was obtained from the MUTH MC production run by the reweighting techniques. The curves are the counter map of $\ln P_{NPT}(E^*, V^*; T^*, P^*) = -6$, -8, -10, -12, and -14 and the outermost curve corresponds to -14.

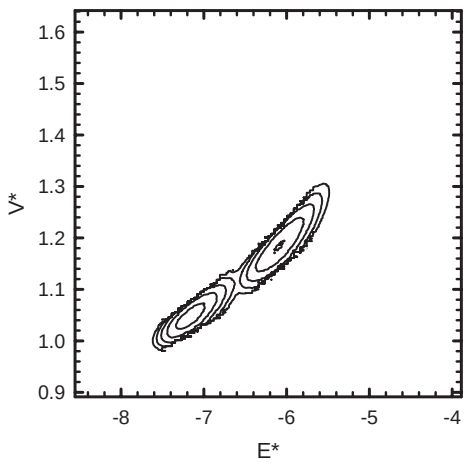

Figure 9. The contour representation of the probability distributions $P_{NPT}(E^*, V^*; T^*, P^*)$ in logarithmic scale at transition temperature $T_c^* = 0.726$ under $P^* = 2.42 \times 10^{-3}$ that was obtained from the MUTH MC production run by the reweighting techniques. The curves are the counter map of $\ln P_{NPT}(E^*, V^*; T^*, P^*) = -6$, -8, -10, -12, and -14 and the outermost curve corresponds to -14.

tities that we calculated for the temperature range between $T^* = 0.417$ and 1.00 suggested that a first-order phase transition is observed at $T_c^* = 0.726$ and the radial distribution functions at below T_c^* ($T^* = 0.417$) and above T_c^* ($T^* = 0.835$) implies that the transition takes place between liquid and solid states.

Adopting parameters for Lennard–Jones argon, the transition temperature is 87 K, differing by 3 K from the experimental data and the differences in enthalpy and entropy at transition temperature agreed well with the experimental data. As far as we know, the present work is the first example of a single simulation run that sampled both liquid state and solid state in isobaric conditions.

The present work was supported, in part, by the Chukyo University Research Fund and by the Ministry of Education, Culture, Sports, Science and Technology (MEXT), Japan: C. M. by Grants-in-Aid for Young Scientists (B), Grant No. 16740244 and Y. O. by Grants-in-Aid for the Next Generation Super Computing Project, Nanoscience Program and for Scientific Research in Priority Areas, Water and Biomolecules.

References

1 B. A. Berg, T. Neuhaus, *Phys. Lett. B* **1991**, *267*, 249.
2 B. A. Berg, T. Neuhaus, *Phys. Rev. Lett.* **1992**, *68*, 9.
3 B. A. Berg, T. Celik, *Phys. Rev. Lett.* **1992**, *69*, 2292.
4 U. H. E. Hansmann, Y. Okamoto, *J. Comput. Chem.* **1993**, *14*, 1333.
5 Y. Okamoto, U. H. E. Hansmann, *J. Phys. Chem.* **1995**, *99*, 11276.
6 W. Janke, S. Kappler, *Phys. Rev. Lett.* **1995**, *74*, 212.
7 N. B. Wilding, *Phys. Rev. E* **1995**, *52*, 602.
8 B. A. Berg, W. Janke, *Phys. Rev. Lett.* **1998**, *80*, 4771.
9 K. K. Bhattacharya, J. P. Sethna, *Phys. Rev. E* **1998**, *57*, 2553.
10 H. Liang, H. Chen, *J. Chem. Phys.* **2000**, *113*, 4469.
11 C. Muguruma, Y. Okamoto, M. Mikami, *Internet Electron. J. Mol. Des.* **2002**, *1*, 583.
12 B. A. Berg, *Comput. Phys. Commun.* **2002**, *147*, 52.
13 E. Bittner, W. Janke, D. B. Saakian, *Phys. Rev. E* **2003**, *67*, 016105.
14 B. A. Berg, *Comput. Phys. Commun.* **2003**, *153*, 397.
15 C. Muguruma, Y. Okamoto, M. Mikami, *J. Chem. Phys.* **2004**, *120*, 7557.
16 C. Muguruma, Y. Okamoto, M. Mikami, *Croat. Chem. Acta* **2007**, *80*, 203.
17 B. A. Berg, *Fields Inst. Commun.* **2000**, *26*, 1.
18 A. Mitsutake, Y. Sugita, Y. Okamoto, *Pept. Sci.* **2001**, *60*, 96.
19 A. M. Ferrenberg, R. H. Swendsen, *Phys. Rev. Lett.* **1988**, *61*, 2635; **1989**, *63*, 1658.
20 A. Rytkönen, S. Valkealahti, M. Manninen, *J. Chem. Phys.* **1998**, *108*, 5826.
21 S. Kirkpatrick, C. D. Gelatt, Jr., M. P. Vecchi, *Science* **1983**, *220*, 671.
22 H. Okumura, Y. Okamoto, *J. Phys. Soc. Jpn.* **2004**, *73*, 3304.
23 H. Okumura, Y. Okamoto, *Phys. Rev. E* **2004**, *70*, 026702.
24 H. Okumura, Y. Okamoto, *Chem. Phys. Lett.* **2004**, *391*, 248.
25 B. A. Berg, *Nucl. Phys. B-Proc. Suppl.* **1998**, *63*, 982.
26 A. M. Ferrenberg, R. H. Swendsen, *Phys. Rev. Lett.* **1989**, *63*, 1195.
27 S. Kumar, J. M. Rosenberg, D. Bouzida, R. H. Swendsen, P. A. Kollmann, *J. Comput. Chem.* **1992**, *13*, 1011.
28 N. Metropolis, A. W. Rosenbluth, M. N. Rosenbluth, A. H. Teller, E. Teller, *J. Chem. Phys.* **1953**, *21*, 1087.
29 G. C. Maitland, M. Rigby, E. B. Smith, W. A. Wakeham, *Intermolecular Forces: Their Origin and Determination*, Clarendon Press, Oxford, **1981**.
30 *American Institute of Physics Handbook*, ed. by D. E. Gray, McGraw-Hill, New York, **1972**.